The Transient Response of Ice Shelf Melting to Ocean Change

PAUL R. HOLLAND

British Antarctic Survey, Cambridge, United Kingdom

(Manuscript received 4 April 2017, in final form 3 June 2017)

ABSTRACT

Idealized modeling studies have shown that the melting of ice shelves varies as a quadratic function of ocean temperature. However, this result is the *equilibrium response*, derived from steady ice–ocean simulations subjected to a fixed ocean forcing. This study considers instead the *transient response* of melting, using unsteady simulations subjected to forcing conditions that are oscillated with a range of periods. The results show that the residence time of water in the subice cavity offers a critical time scale. When the forcing varies slowly (period of oscillation $\gg$ residence time), the cavity is fully flushed with forcing anomalies at all stages of the cycle and melting follows the equilibrium response. When the forcing varies rapidly (period $\leq$ residence time), multiple cold and warm anomalies coexist in the cavity, cancelling each other in the spatial mean and thus inducing a relatively steady melt rate. This implies that all ice shelves have a maximum frequency of ocean variability that can be manifested in melting. Between these two extremes, an intermediate regime occurs in which melting follows the equilibrium response during the cooling phase of the forcing cycle, but deviates during warming. The results show that ice shelves forced by warm water have high melt rates, high equilibrium sensitivity, and short residence times and hence a short time scale over which the equilibrium sensitivity is manifest. The most rapid melting adjustment is induced by warm anomalies that are also saline. Thus, ice shelves in the Amundsen and Bellingshausen Seas, Antarctica, are highly sensitive to ocean change.

1. Introduction

The glacial ice sheets of Greenland and Antarctica are losing mass, contributing to sea level rise (Shepherd et al. 2012). In Antarctica, the majority of this mass loss is caused by ice adjustment to change in ocean melting of the floating ice shelves (Shepherd et al. 2004). Antarctic ice shelves are subject to a range of different ocean forcing regimes (Jenkins et al. 2016), each with distinct modes of variability.

The Filchner–Ronne Ice Shelf (FRIS) in the Weddell Sea is an example of a large ice shelf melted by relatively cold waters. Cold and saline High Salinity Shelf Water at approximately −1.8°C (the surface freezing point), formed by intense sea ice growth, forces the large FRIS cavity (Nicholls et al. 2009), leading to low melt rates $O(0.1)$ m yr^{-1} (Makinson et al. 2011). Wintertime ice growth forces the cavity with variable annual pulses of cold, saline water, which recirculate around the cavity with an estimated mean residence time of 4–5 years (Nicholls and Østerhus 2004). Warmer and fresher Modified Warm Deep Water is also present offshore, with temperatures up to −1.3°C (Nicholls et al. 2008, 2009), and a model study indicates the possibility that this water may in the future intrude into the cavity, increasing melt rates by at least an order of magnitude (Hellmer et al. 2012). Such an outcome would severely compromise the stability of FRIS and therefore the West Antarctic Ice Sheet.

The smaller ice shelves in the Amundsen Sea are melted by warmer waters. Sea ice growth is less intense in the Amundsen Sea (Petty et al. 2013), allowing warm and saline Circumpolar Deep Water at approximately 1°C to flood the continental shelf and occupy its ice shelf cavities (Jacobs et al. 2012). These ice shelves melt at mean rates of $O(10)$ m yr^{-1} and hence are much smaller than FRIS, responding to ocean changes on a time scale of only a few months (Heimbach and Losch 2012). Most of Antarctica's sea level contribution is caused by thinning and acceleration of the ice streams discharging into the Amundsen Sea (Konrad et al. 2017; Mouginot et al. 2014) in response to increased ocean melting. Ocean melting may have been anomalously rapid in recent decades, thinning ice streams that were previously in balance with slower melting. However, the ocean forcing varies significantly on a wide range of time scales,

Corresponding author: Paul R. Holland, p.holland@bas.ac.uk

DOI: 10.1175/JPO-D-17-0071.1

from seasonal to decadal, and no simple warming trend is evident (Christianson et al. 2016; Dutrieux et al. 2014; Jenkins et al. 2016; Webber et al. 2017). Ongoing ice stream thinning may instead be dominated by a coupled ice–ocean instability triggered by historical decadal ocean variability (Jenkins et al. 2016; Smith et al. 2016).

These examples illustrate the importance of the response of ice shelf melting to unsteady ocean forcing. This study seeks to understand this response over the full range of observed conditions, for which the above examples represent end members. Performing a series of idealized simulations, Holland et al. (2008) established that ice shelf melting generally increases as a quadratic function of ocean temperature. This occurs because the meltwater-driven circulation accelerates as the ocean warms. The simulations showed that both the heat available for melting and the turbulence driving the ocean to ice heat flux are increased linearly as the ocean warms, so the melt rate increases quadratically because it is proportional to the product of these two quantities. This result is obtained from a set of simulations, each forced by a different far-field ocean temperature and run until the melting becomes steady. The quadratic curve is the relationship between the set of steady-state melt rates and the set of simulation forcing temperatures. This curve is here referred to as the *equilibrium response* of ice shelf melting to ocean temperature perturbation.

In contrast, the present study seeks to establish the full *transient response* of ice shelf melting to ocean perturbations, using simulations with unsteady forcing. In each simulation, an idealized subice shelf ocean domain is forced by oscillating far-field ocean conditions. Different simulations span a wide range of oscillation periods. Within each simulation, the relationship between melting and ocean forcing is examined as a function of time.

2. Method

a. Model

The ocean model is the MITgcm checkpoint c65t, with a grid of $dz = 20\,\text{m}$ resolution in the vertical and $dx = dy = 1\,\text{km}$ in the horizontal. The model is hydrostatic and Boussinesq, with an implicit nonlinear free-surface scheme and a third-order direct space–time, flux-limited advection scheme. Free-slip boundary conditions are used on the sidewalls and a quadratic drag with coefficient 0.0025 is used on the seabed. The equations are solved on an f plane with $f = -1.4 \times 10^{-4}\,\text{s}^{-1}$. A linear equation of state is used, with thermal expansion coefficient $\alpha = 3.9 \times 10^{-5}\,^{\circ}\text{C}^{-1}$ and haline contraction coefficient $\beta = 7.41 \times 10^{-4}$ chosen specifically to control the density perturbation associated with a given thermal and haline forcing (see below). Constant viscosities and diffusivities are used, with values of 50 and $10\,\text{m}^2\,\text{s}^{-1}$ in the horizontal and 10^{-3} and $10^{-4}\,\text{m}^2\,\text{s}^{-1}$ in the vertical, respectively. Partial cells are used to better represent the sloping ice base, with a minimum open-cell fraction of 0.1. A time step of 60 s is used throughout. Convective adjustment removes unstable stratification every time step.

Ice shelf melting is implemented using the ''three-equation'' approach calibrated against observations by Jenkins et al. (2010). Specifically, values of $C_d = 0.0097$, $\Gamma_T = 0.011$, and $\Gamma_S = 3.1 \times 10^{-4}$ are used for the drag coefficient and the turbulent heat and salt exchange coefficients, respectively, and the conductive heat flux into the ice shelf uses an internal ice temperature of -20°C. Thermal and haline driving and free-stream velocity are calculated using temperatures, salinities, and velocities averaged over a distance of dz (the vertical grid resolution) from the ice; because of the use of partial cells, this generally involves two cells in the vertical (Losch 2008). In a modification to the basic code, the velocities are averaged vertically over the distance dz at each velocity point, and then the four velocity averages on the sides of each tracer cell are averaged together to calculate the friction velocity and hence melting at tracer points. This ensures that no zero flow values are averaged into the friction velocity when tracer cell sidewalls are partially ice. A minimum current speed of $10^{-6}\,\text{m}\,\text{s}^{-1}$ in the friction velocity ensures that melting never stagnates. To avoid thin partial cells becoming too cold or fresh, virtual heat and salt fluxes are applied to the top dz of the water column, in a conservative manner (Jenkins et al. 2001; Losch 2008). Quadratic drag with $C_d = 0.0097$ is applied to ocean currents at the ice base.

b. Experimental design

The domain consists of a simple, wedge-shaped ice shelf in a cuboid ocean (Fig. 1). The ice shelf is 50 km by 50 km wide with a draft sloping from 900 to 200 m deep. The ocean is 1000 m deep, 50 km wide, and 150 km long. The only external forcing applied is the restoring of ocean temperature and salinity at the boundary opposite the ice shelf. The restoring is applied progressively, with strong restoring at the wall (time scale 1 day), weakening linearly to no restoring 10 km from the wall.

A variety of ocean restoring conditions are used to elucidate the equilibrium and transient responses of the model to imposed ocean change. Five different classes of simulations are performed, each illustrating a different concept. Within each class, a set of equilibrium simulations are performed, with steady ocean restoring

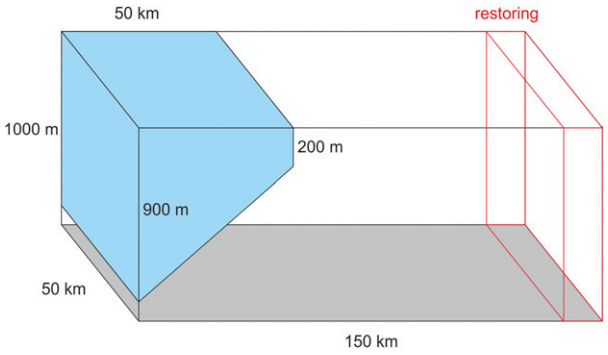

FIG. 1. Domain and forcing of the idealized experiments. The domain consists of a simple, wedge-shaped ice shelf in a cuboid ocean. The sole external forcing on the ocean is a restoring zone on the boundary opposite the ice shelf, and the balance between this restoring and the ice shelf heat and freshwater fluxes determines the ocean behavior.

conditions. These simulations are run to steady state, and the set of melt rates from the steady simulations defines the equilibrium response. A series of transient simulations are also performed for each class. These simulations use oscillating ocean restoring conditions, with a wide range of oscillation periods, to probe the transient response of the model. Oscillating forcings are repeated until the model is spun up into a repeating state, whereupon the final cycle is analyzed. All simulations are initialized using ocean conditions from the "warmest" phase of the oscillating forcing to minimize spinup time (see below). It is simplest to introduce the forcing used in each simulation class alongside the results.

3. Reference simulations

a. Simulation design

The reference (REF) class consists of a highly idealized, extreme forcing selected to emphasize the mechanisms underlying the transient response (Fig. 2). The temperature profile varies from a fixed, cold (−1.8°C) surface layer of 200-m depth, over a variable thermocline 200 m thick, to a deep ocean with variable ocean temperature. The REF class simulations include five equilibrium simulations with steady deep-ocean temperatures at −1.8°, −1°, 0°, 1°, and 2°C and six transient simulations with deep-ocean temperatures that oscillate between −1.8° and 2°C using repeating sine waves with periods of 0.25, 0.5, 1, 2, 5, and 10 years. All REF class simulations have a salinity profile that is fresh in the surface layer and saline at depth, leading to a strong pycnocline because salinity controls density. Crucially, the deep forcing salinity is deliberately varied between 34.3 and 34.5 as the deep temperature oscillates from cold to warm. With the coefficients selected in the linear equation of state, these salinity changes exactly offset all density variations

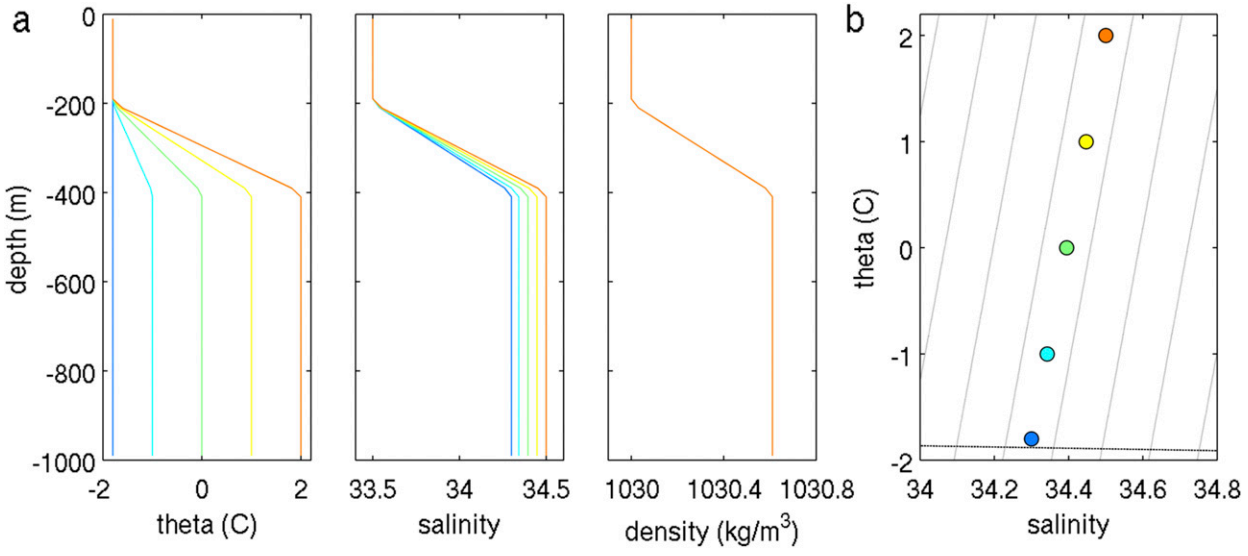

FIG. 2. Ocean restoring conditions in REF simulations. (a) Profiles of potential temperature, salinity, and potential density. The deep-ocean temperature and salinity are varied simultaneously to provide a variable temperature but constant density forcing on the ocean. (b) Potential temperature–salinity diagram of the evolution of the deep-ocean forcing (beneath 400 m). Gray lines are isopycnals, and the dotted black line is the freezing temperature. In all panels, the colored lines and dots show the steady forcing used in equilibrium simulations. The cyclic forcing used in transient simulations varies back and forth through these values in a continuous sine wave. The use of a linear equation of state and carefully chosen conditions mean that the deep-ocean temperature variation occurs along an isopycnal, and the density profile is therefore steady.

due to temperature, leading to a steady boundary forcing density (Fig. 2). This is referred to hereinafter as *density compensation*. In consequence, density variations within REF simulations are solely forced by ice shelf melting, not by ocean boundary forcing.

b. Equilibrium response

To understand the transient response, it is first necessary to examine the equilibrium response. Figure 3 shows the steady-state ocean conditions for two of the equilibrium simulations (deep-ocean forcing temperatures of −1.8° and 1°C). The melt rates show high melting on the Coriolis-favored side of the ice shelf, which is the result of high friction velocity and thermal driving within a rapid meltwater current trapped against the sidewall of the domain (Dansereau et al. 2014; Determann and Gerdes 1994; Stern et al. 2014). Relatively high melt rates and no regions of freezing occur in these simulations, as a result of the relatively steep slope of the ice base (Lazeroms et al. 2017). The melt rates also show clear "stripes" running across the slope, which are primarily the result of velocity artifacts caused by the stepped ice base in the Cartesian coordinates used here, despite the use of partial cells and a modified boundary layer scheme to reduce this problem. Melting is approximately 20 times higher in the warm case.

The ocean circulation is significantly faster in the warm case. Flow immediately beneath the ice is approximately 5 times faster, contributing to the melting increase, and the general circulation in the open ocean is an order of magnitude faster. In all cases, the barotropic circulation is more vigorous than the overturning circulation (not shown), so the circulation is primarily horizontal, and the barotropic circulation in the open ocean is more vigorous than that in the subice cavity.

Both cases feature water at the restoring temperature and salinity on the boundary, with a cold and fresh meltwater current rising up the base of the ice and intruding out into the open ocean within and below the pycnocline. In the cold case, the meltwater is colder than the surface freezing temperature as a result of the pressure depression of the freezing temperature at the deep ice base. The warm case is generally more saline due to its density-compensated forcing.

The buoyant subice meltwater currents are visible in Fig. 3 in both the velocity vectors and temperature and salinity sections. The first baroclinic Rossby radius is ~5 km in this model setup, so the meltwater flow is resolved horizontally by the model resolution of 1 km. The Ekman layer depth beneath the ice shelf is only ~4 m in this model, so the spiral current structure is not represented by the 20-m vertical resolution. However, Jenkins (2016) shows that the meltwater current structure is dictated by the buoyancy perturbation, which can extend over a greater depth. In the model, the meltwater is input over a depth dz, and buoyancy and velocity are equally resolved, so the interplay between them is captured. Thus, the representation of the meltwater current is expected to be qualitatively correct even if the buoyant layer is quantitatively too thick.

Figure 4 shows the equilibrium response of the REF class simulations. For each of the five equilibrium simulations, the steady area-mean ice shelf melt rate at the end of the simulation is plotted against the deep-ocean forcing temperature. As discussed by Holland et al. (2008), the equilibrium response follows a quadratic curve. This has the important implication that ice shelves forced by warmer water not only have higher melt rates but also have a greater sensitivity of melt rates to temperature change.

To understand the transient response, it is useful to first consider within these equilibrium results the time scale over which ocean forcing anomalies might be expected to influence melting. Anomalies from the forcing boundary will rapidly traverse the open ocean (Fig. 3), and the slower barotropic circulation beneath the ice will then limit the rate at which they flush the cavity waters and affect melting. It is straightforward to combine the flux across the ice front with the cavity volume to calculate a cavity residence time (Table 1). (The minimum barotropic streamfunction along the ice front is virtually identical to the full flux across the ice front, that is, the circulation is nearly barotropic.) However, within the cavity, the area close to the ice front and on the Coriolis-favored side is much more rapidly flushed than the remainder (Fig. 3), and all cavity waters must be flushed with an ocean temperature anomaly for it to be fully reflected in the area-mean melt rate. Therefore, it is more representative to define the *mean cavity residence time*, which is the cavity volume divided by the area mean of the barotropic streamfunction within the cavity. The mean cavity residence time is approximately 4 times longer than the ice front flux residence time (Table 1). By any measure, the simulations forced by the coldest water have a significantly longer residence time than all other temperatures, and this difference will prove important to the nature of the transient response.

c. Transient response

Figure 5 shows the transient response of the unsteady simulations in the REF class. Specifically, this figure shows how the area-mean ice shelf melt rate evolves in time as the ocean forcing temperature is varied. The colored dots represent a spunup cycle from the transient simulation in question, while the black dots and gray line show the REF class equilibrium response (Fig. 4) for

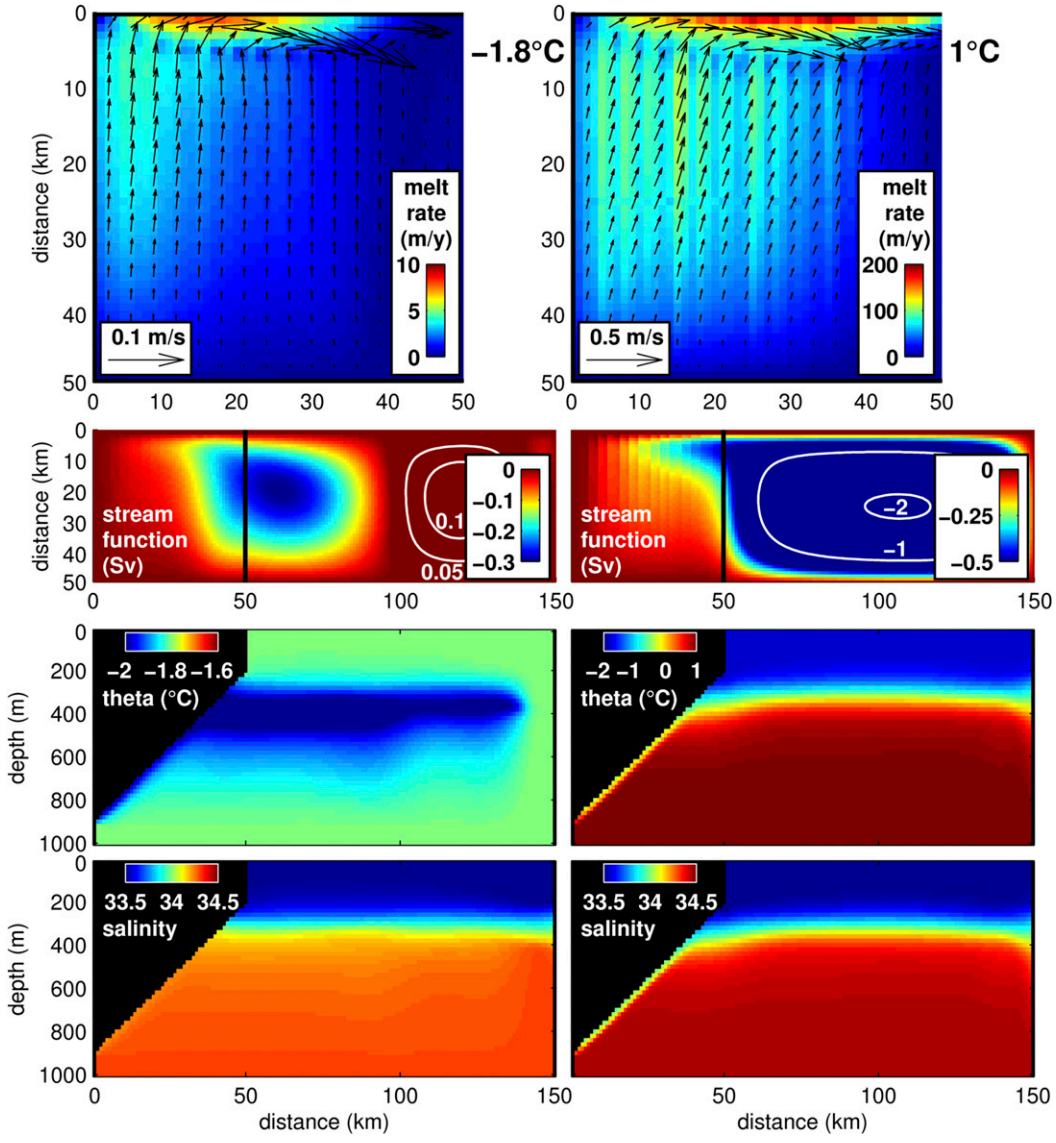

FIG. 3. Ocean properties in steady state for illustrative (left) cold and (right) warm equilibrium simulations from the REF class. In all panels the grounding line is on the left side of the figure. The top row shows a plan view of ice melting and flow in the ice–ocean boundary layer (vectors shown every third grid point); stripelike features are clearly visible as a result of the Cartesian coordinate system. The second row shows a plan view of the barotropic streamfunction, with the ice front position marked by a black line. The color scale focuses on the streamfunction within the cavity, while labeled white contours show the stronger circulation in the open ocean. The third and fourth rows show vertical sections of potential temperature and salinity, respectively, along the center of the domain.

comparison. The coloring of the dots signifies the passage of time within each forcing cycle; each cycle progresses from its warmest forcing (blue), to its coldest forcing (green), and back to its initial warm forcing (red). Each panel shows the results from a different simulation, with the ocean forcing oscillating with a different period. As might be expected, for slowly varying forcing, the transient response stays close to the equilibrium response, but as the forcing is varied more rapidly, the melting deviates from the equilibrium curve.

For an ocean temperature anomaly to affect melting, the water bearing that anomaly must be flushed through the cavity. The equilibrium melt rate is achieved when the cavity is filled with water that is exactly in balance with the steady forcing properties. However, when the forcing properties are varying in time, the cavity can never fully achieve this state. The proximity

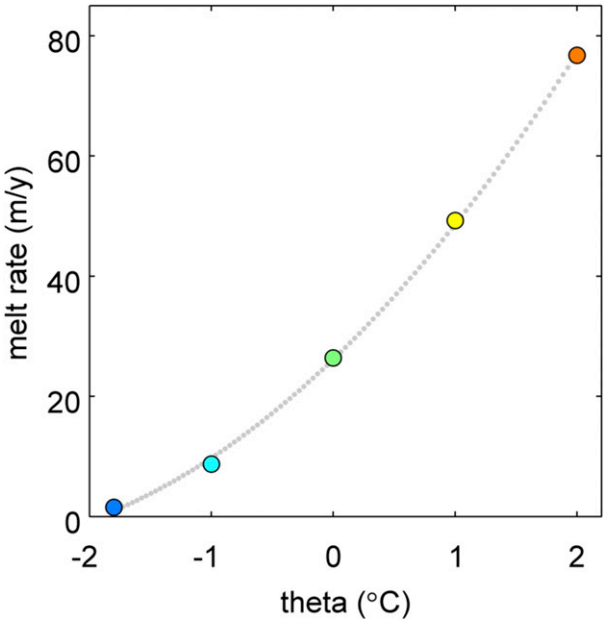

FIG. 4. Equilibrium response of the steady cases in the REF class. Each dot marks the area-mean ice shelf melt rate from the steady state of a single simulation, plotted against the deep-ocean forcing temperature for that simulation. The colors of the dots correspond to the forcings shown in Fig. 2. The gray dotted line illustrates the best-fit quadratic curve (Holland et al. 2008).

of the cavity state to its equilibrium state is determined by the rate of flushing relative to the rate of forcing variation. Consider a case in which the period of the forcing variation is 10 times longer than the mean cavity residence time. In that case, the cavity waters will be flushed 10 times during each forcing oscillation, and the cavity waters will thus fully reflect each 10% of the forcing signal. As a result, we might expect that the transient melt rate will remain within approximately 10% of the equilibrium response. Considering our mean cavity residence times of 0.3–0.5 years (Table 1), this suggests that forcing varying more slowly than a 3–5-yr period will remain within approximately 10% of the equilibrium response. The results are broadly in agreement with this (Fig. 5); an exact match cannot be expected, since the circulation causes the cavity to have a range of residence times (Fig. 3). Slower-varying forcing will be closer to equilibrium, as the cavity is flushed more times during each forcing cycle and so cavity waters will better reflect all phases of the forcing.

Next consider that the coldest phase of the forcing cycle takes longest to flush, since the cold-water regime has the slowest circulation and hence the longest residence time of 0.5 years (Table 1). Thus, a 5-yr period forcing cycle might be expected to induce melt rates within 10% of the equilibrium response during the cold phase. Conversely, the warmest phase of the forcing is quickest to flush, since the warm-water regime has the fastest residence time of 0.3 years; a 3-yr cycle might have melt rates within 10% of equilibrium. Therefore, as the forcing period is shortened, the cold phase of the cycle will depart significantly from equilibrium sooner than the warm phase. The results broadly bear out this simple narrative (Fig. 5). The simulation with a 5-yr period (greater than 10 times the warm residence time but not the cold residence time) stays close to the equilibrium result while the cavity remains relatively warm, that is, while the forcing is cooling down (blue to green dots in Fig. 5). However, once the cavity is cold, the circulation decelerates and the cavity residence time increases. The result is that when the forcing is warming back up (green to red dots) the cavity is not flushed with the warming water as rapidly, and the melt rate strays further from its equilibrium value. This asymmetry is also seen in shorter-period simulations.

Simulations with forcing periods of less than 3 years have forcing changing more rapidly than 10 times the mean cavity residence time even at the warmest forcing phase, and melting deviates from the equilibrium curve throughout the cycle. One important feature is that for short forcing periods the amplitude of the melting

TABLE 1. Ice shelf cavity fluxes and residence times calculated for the steady equilibrium simulations in the REF class. The coldest case has a significantly slower circulation than the other simulations and thus a longer residence time. For all cases, the flux across the ice front does not fully reflect the flushing of the cavity, since the fastest flow does not flush the farthest reaches of the cavity (Fig. 3). Therefore, a more representative mean cavity flushing flux (and residence time) is calculated from the area mean of the cavity barotropic streamfunction. Residence times are calculated using the cavity volume of $\sim 10^{12}\,m^3$.

Simulation	Barotropic ice front flux (Sv)	Ice front flux residence time (yr)	Mean cavity barotropic streamfunction (Sv)	Mean cavity residence time (yr)
REF −1.8°C	0.27	0.12	0.07	0.50
REF −1°C	0.45	0.07	0.11	0.31
REF 0°C	0.47	0.07	0.10	0.32
REF 1°C	0.49	0.07	0.10	0.32
REF 2°C	0.52	0.06	0.11	0.30

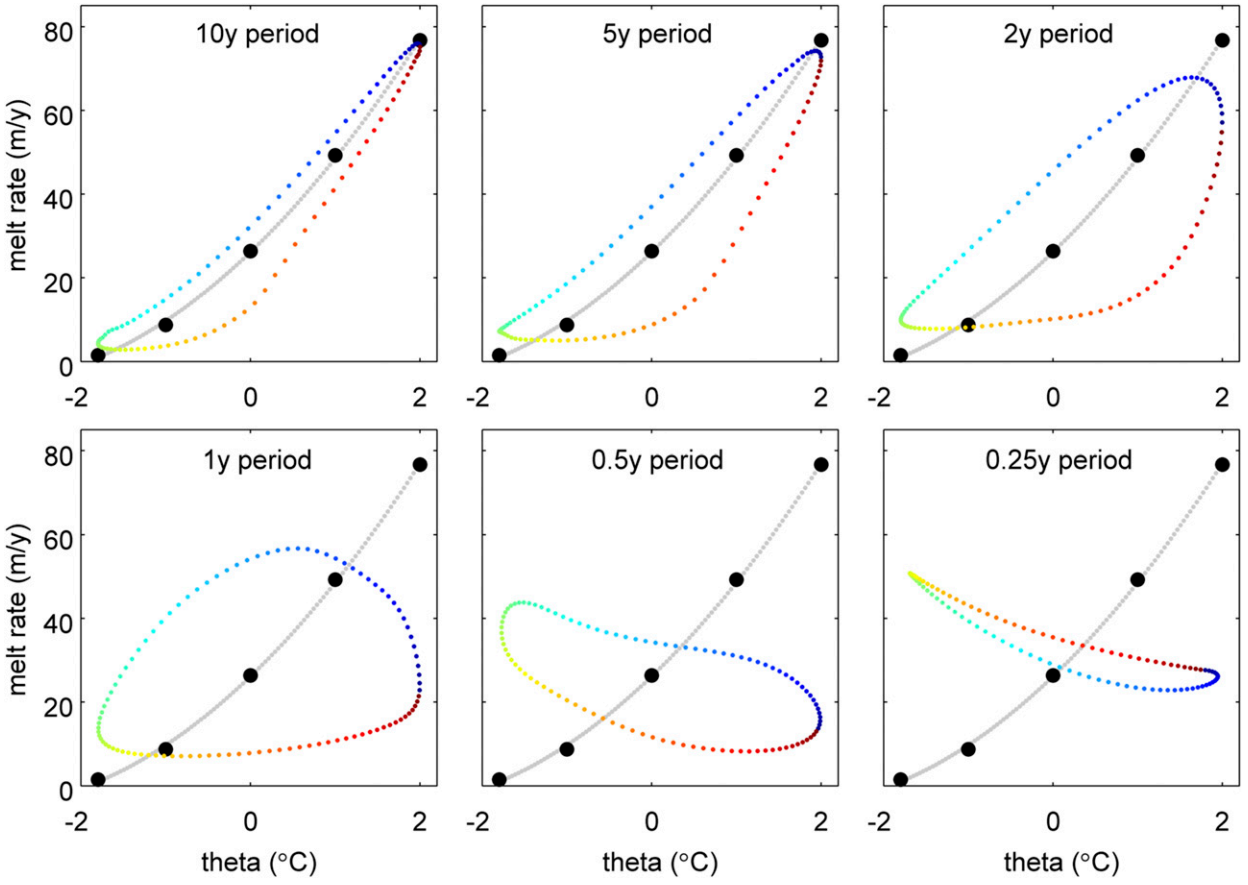

FIG. 5. Equilibrium and transient responses of simulations in the REF class. Each panel represents the evolution of a different transient simulation, each with ocean forcing conditions oscillating with a different period. The colored dots represent the time evolution of the area-mean ice shelf melt rate, as a function of the deep-ocean forcing temperature, over a single cycle of the forcing after the model is spun up into a repeating state. The coloring of the dots signifies the passage of time within each cycle, progressing from the warmest forcing (blue dots), to the coldest forcing (green dots), and back to the warmest forcing (red dots). The same number of dots is shown in each panel despite the large difference in time period. For reference, the black dots and gray dotted line show the equilibrium response from the steady simulations, as shown in Fig. 4. For ocean forcing conditions that evolve slowly, the transient response stays close to the equilibrium response. As the forcing oscillation period gets shorter, the equilibrium and transient responses differ significantly.

response is significantly reduced. When the forcing is oscillated so rapidly that warm and cold anomalies coexist in the cavity, these anomalies compensate each other in the spatial-mean melt rate. In the limiting case that many anomalies coexist, the melt rate conceptually tends to a steady rate equaling the melt rate produced by the mean forcing temperature. Such compensation should start to occur when the forcing period equals the cavity residence time, since then a single warm and cold anomaly occur within each flushing of the cavity. Indeed, the simulations show that the amplitude of the melting oscillations is significantly reduced when the period of forcing approaches the mean cavity residence time of 0.3–0.5 years (Fig. 5). Thus, the mean residence time characterizes a critical cutoff period for each ice shelf; ocean variability more rapid than this is not fully manifested in the shelf-averaged melt rate.

Another notable effect within the short-period cases is that the melting goes out of phase with the forcing, with the most rapid melting occurring during the cold phase. This arises from the delay inherent in the requirement that the circulation flush ocean anomalies through the cavity. Melting anomalies might be expected to be determined by a backward-in-time average of ocean forcing anomalies over the duration of the mean cavity residence time. This implies a lag of half of the residence time, 0.15–0.25 years in our simulations, as observed in the results (Fig. 5).

All of these effects are also visible within melting time series (Fig. 6). These figures show the predicted equilibrium response in gray, and the transient response in color, as in Fig. 5. The time axis shows the period over which the results for Figs. 5 and 6 are taken. The

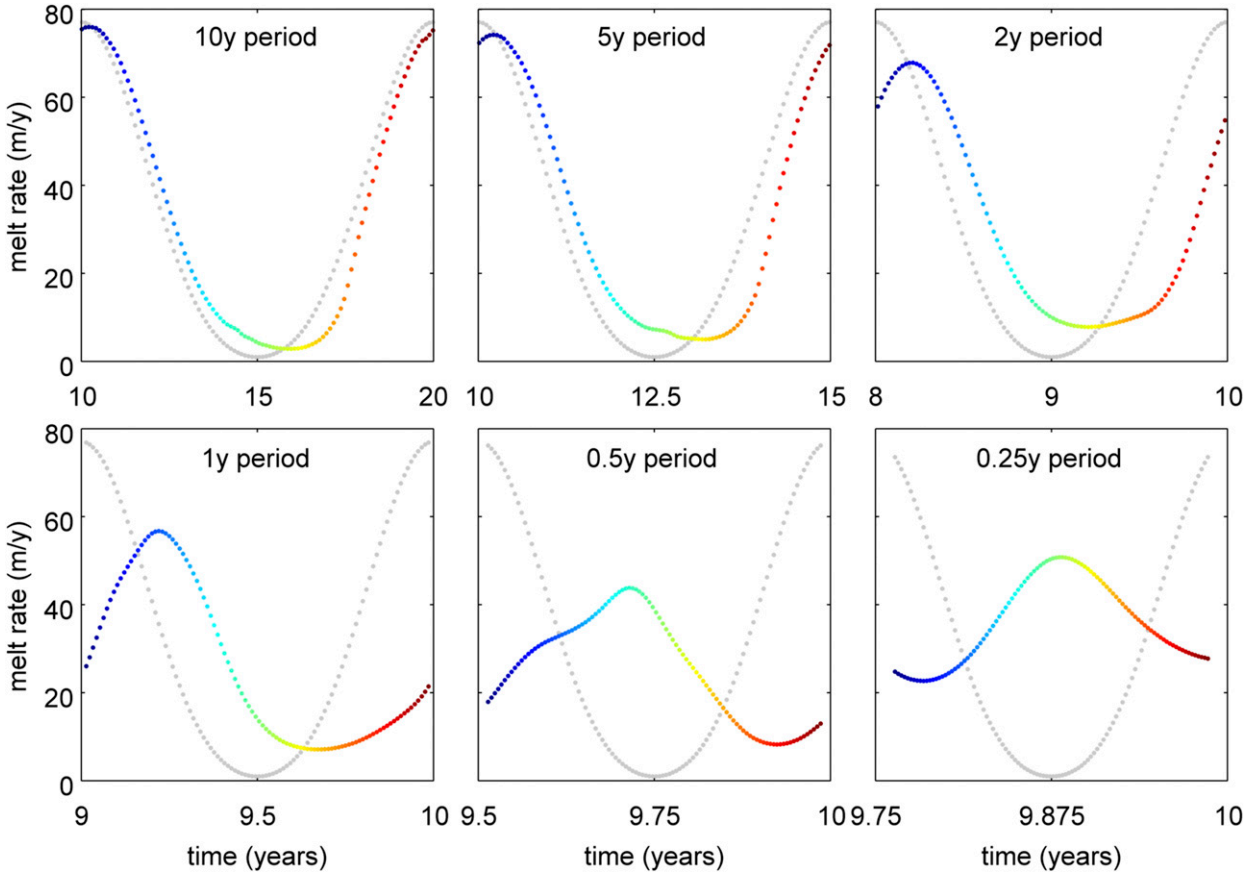

FIG. 6. Time evolution of the unsteady cases in the REF class. Colored dots represent the time evolution of the area-mean ice shelf melt rate, as shown in Fig. 5, after the model is spun up into a repeating state. For reference, the gray dots indicate the melting variation predicted by the equilibrium response. This prediction is derived by applying the quadratic melt–temperature relationship to the oscillating forcing temperature. As the oscillation period decreases, the lag between the forcing and response becomes more significant, and the amplitude of the melting oscillation decreases.

predicted equilibrium response is calculated by inserting the oscillating forcing temperature into the quadratic melting–temperature relation shown in Figs. 4 and 5. Figure 6 clearly shows how for longer-period runs, the lag between the equilibrium prediction and full transient response is persistently more apparent during the cold phase of the forcing. For shorter-period runs the melting anomaly amplitude is reduced, and the signal goes out of phase with the equilibrium prediction.

4. Further simulations

a. Uncompensated density changes

The effect of density compensation in the forcing is next examined using a set of simulations that are similar to REF but with varying degrees of density compensation, referred to as the UNCOMP class. All UNCOMP simulations use the same temperature forcing as REF and a fixed 5-yr period of oscillation. However, the different UNCOMP transient simulations each have deep-ocean forcing salinities oscillating over a different range to provide an unsteady forcing density (Fig. 7, top row). In all UNCOMP simulations, the salinity is fixed at 34.3 when the temperature is at the coldest phase of its oscillation, but different salinities are assigned to the warmest phase of the oscillation. Simulations with warm-phase salinities of 34.3, 34.5, 34.7, and 34.9 are performed. In the 34.3 simulation, the deep-ocean forcing salinity is steady, so the thermally induced density change is not offset, and the forcing profile becomes more buoyant when it is warmer. The 34.5 simulation is perfectly density-compensated, corresponding to the 5-yr period REF simulation discussed above. In the 34.7 and 34.9 simulations, the forcing is more saline (denser) when it is warmer. All equilibrium results shown are density-compensated simulations from the REF class.

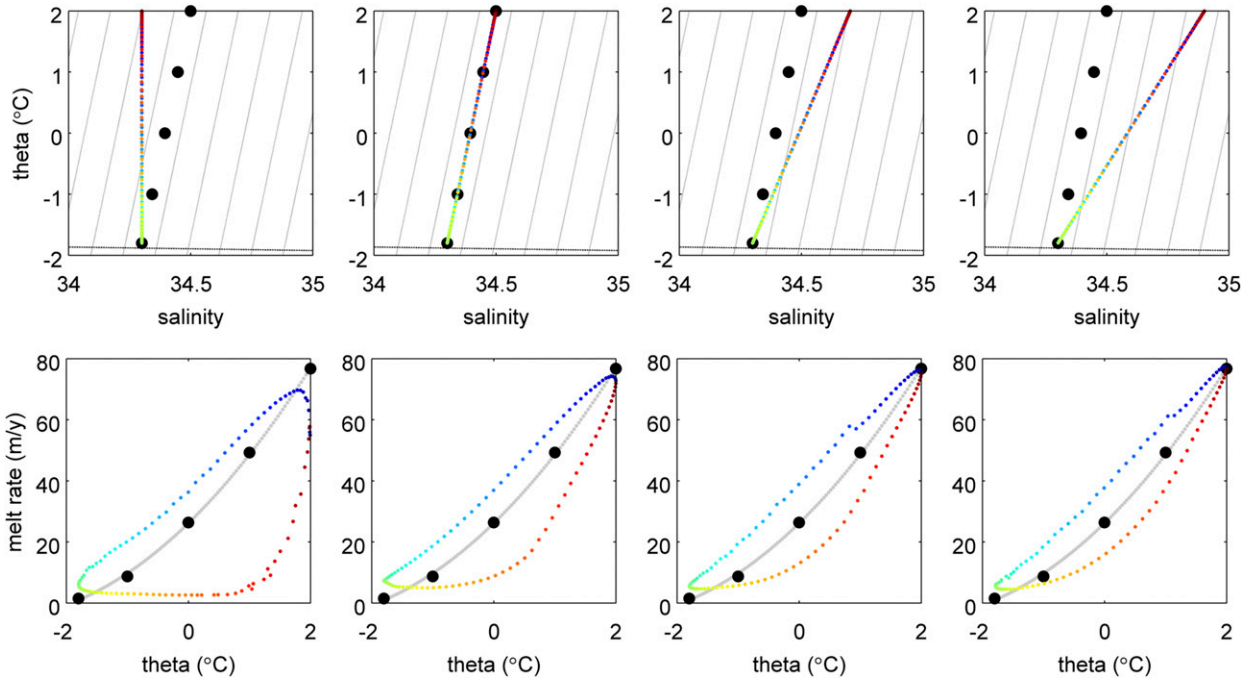

FIG. 7. Equilibrium and transient responses of simulations in the UNCOMP class. Each column represents a simulation with a different level of density compensation in the forcing, all with forcing conditions oscillating over a 5-yr period. (top) The evolution of the deep-ocean forcing in temperature–salinity space, where light gray lines are isopycnals and the dark gray line is the freezing point. (bottom) The transient response of melting for these simulations, as in Fig. 5. The simulations transition from (first column) the warm phase of the oscillation being more buoyant, through (second column) density compensation, to (third and fourth columns) the warm phase being denser. The density-compensated case corresponds to the REF class simulation shown in Fig. 5. All equilibrium results are from the REF class. When the warm anomaly is more buoyant, the deviation of the transient response from the equilibrium response is exacerbated because the buoyant warm water is less effective at displacing cold, denser water occupying the subice cavity.

As discussed in section 3c, the density-compensated case with 5-yr period forcing deviates a little from the equilibrium curve. The mean cavity residence time is longest when cavity waters are cold, so during the warming phase of the forcing there is a delay in the import of the warming signal to the cavity and melting deviates from equilibrium. Density compensation has a significant effect upon this mechanism (Fig. 7, bottom row). In the simulation where warm water is of equal salinity to cold, warm anomalies are more buoyant. Warm anomalies therefore have to work against gravity to displace cold water from the cavity, and the lag in melting recovery is significantly exacerbated. In the simulations where warm water is more saline than cold, dense warm anomalies displace cold water more readily, and the lag in melting recovery is relieved.

These results demonstrate an important principle. In the Amundsen Sea, warm Circumpolar Deep Water is also the most saline water on the shelf. Therefore, warm anomalies are saline and thus highly effective at penetrating ice shelf cavities and affecting melt rates. In the Weddell Sea, Modified Warm Deep Water is warmer, but also fresher, than the cold High Salinity Shelf Water from which FRIS cavity waters are derived. Therefore, warm anomalies are fresh and far less effective at altering melt rates because they must work against gravity to enter the cavity.

Another feature visible in Fig. 7 are slight ''kinks'' in the evolution of melting as a function of temperature, which is caused by the lack of density compensation. When the boundary density forcing is strong and varying in time, this can produce large horizontal density gradients, which trigger baroclinic instability in this rotating system. This instability sheds eddies from the boundary, and the warm and cold water carried by these eddies induces small melting perturbations.

b. Warm and cold cases

To illustrate the basic mechanisms underlying the transient response, REF and UNCOMP class simulations employ a deep-ocean forcing that oscillates between −1.8° and 2°C. However, this temperature range is clearly unrealistically large and so additional experiments are conducted with a smaller oscillation amplitude. This also permits consideration of the effect of a different mean forcing temperature. WARM and

COLD class simulations both feature ocean temperature forcing that is density compensated and of a similar configuration to the REF class but with deep-ocean temperature varying by just 0.5°C. WARM class simulations have temperatures oscillating between 0.75° and 1.25°C, while COLD class simulations oscillate between −1.8° and −1.3°C. For each of the WARM and COLD classes, three equilibrium simulations are performed (at the minimum, mean, and maximum thermal forcing), and four transient simulations are performed, with oscillation periods of 0.5, 1, 2, and 5 years.

As discussed in section 3b, warm ocean conditions lead to higher melt rates, a higher equilibrium melt rate sensitivity, and a faster ocean circulation. WARM class simulations (Fig. 8, top row) have high melt rates and a steep equilibrium curve (which appears linear). With an oscillation period of 5 years, the WARM class transient simulation closely follows the WARM equilibrium curve. With a period of 0.5 years, the WARM class simulation still displays significant melting variation. These features are explained by the rapid ocean circulation produced by high melt rates. With a short mean cavity residence time, the WARM class can rapidly adjust to ocean temperature perturbations.

Colder ocean conditions lead to lower, less sensitive melt rates and a slower ocean circulation and hence longer cavity residence times. In COLD class simulations (Fig. 8, bottom row), the equilibrium curve is shallower (and visibly nonlinear). Transient simulations with a 5-yr period are far from equilibrium, and simulations with a 0.5-yr period produce a very weak response of melting to ocean temperature variations.

These results highlight several important implications for the transient response of warm- and cold-water ice shelves. First, as shown above, ice shelves do not respond significantly to forcing variations with a period shorter than the mean cavity residence time, so warm-water ice shelves will respond to rapid forcing variations that do not induce any response in cold-water ice shelves. Second, for any given forcing period longer than the residence time, warm-water ice shelves experience a greater melting response than cold-water ice shelves, both in absolute terms and also as a proportion of their equilibrium response. Finally, warm-water ice shelves attain the equilibrium response (the fullest possible response) in transient simulations with a shorter forcing period than cold-water ice shelves.

c. *Pycnocline cases*

So far, all simulations have perturbed the ocean forcing of ice shelf melting by oscillating the deep-ocean temperature and salinity. However, this forcing does not accurately characterize ocean variability in the Amundsen and Bellingshausen Seas, which occurs through the thickening and thinning of a Circumpolar Deep Water layer with relatively steady properties (Dutrieux et al. 2014; Martinson et al. 2008). Therefore, to examine this mode of variability, the CLINE class of simulations uses an ocean forcing with oscillating pycnocline depth. Ocean conditions follow De Rydt et al. (2014), with a top layer of uniform temperature of −1°C and salinity 34 and a bottom layer of 1°C and 34.7, separated by a linear pycnocline 400 m thick. The forcing is varied by shifting the entire pycnocline up and down uniformly, with the top of the pycnocline varying between 200 and 400 m. This varies the thickness of the warm deep layer.

Figure 9 shows the equilibrium and transient responses of the CLINE class simulations, with melting plotted against the depth of the top of the pycnocline rather than deep-ocean temperature. As in WARM simulations (Fig. 8, top row), melt rates are high and the equilibrium sensitivity is approximately linear. However, the model clearly responds much more rapidly to pycnocline oscillation than to variations in deep-water properties; CLINE unsteady cases follow their equilibrium curve when the conditions are subject to an oscillation period as short as 1 year, and an oscillation of only 3 months' period is required to observe a significant deviation from the equilibrium response.

The basic explanation for this rapid response is that the warm anomalies in the CLINE class are accompanied by saline anomalies, and hence warm anomalies are denser. The deep layer is much more saline than the surface layer, so when the pycnocline is elevated at the shallow phase of its cycle, there is a warm and dense anomaly in the forcing as the saline bottom layer is thickened. As expected from the UNCOMP simulations in Fig. 7, when warm anomalies are dense the buoyancy-driven circulation drives the warm water into the cavity, and deviation from the equilibrium response is significantly reduced. This argument can be illustrated by performing a CLINE simulation that is density compensated; the salinity of the deep layer is reduced to 34.11, so that the deep and shallow layers have the same density (Fig. 9). With a 1-yr period of oscillation this simulation is clearly divergent from any equilibrium curve. Thus, the rapid response of melting to transient forcing in the CLINE simulations is explained by (i) the rapid melting (hence short residence time) induced by the relative warmth of the forcing and (ii) the high salinity (density) of warm anomalies in the forcing.

5. Application to real ice shelves

It is important to note the limitations of this idealized study. The study only considers temporal variation in

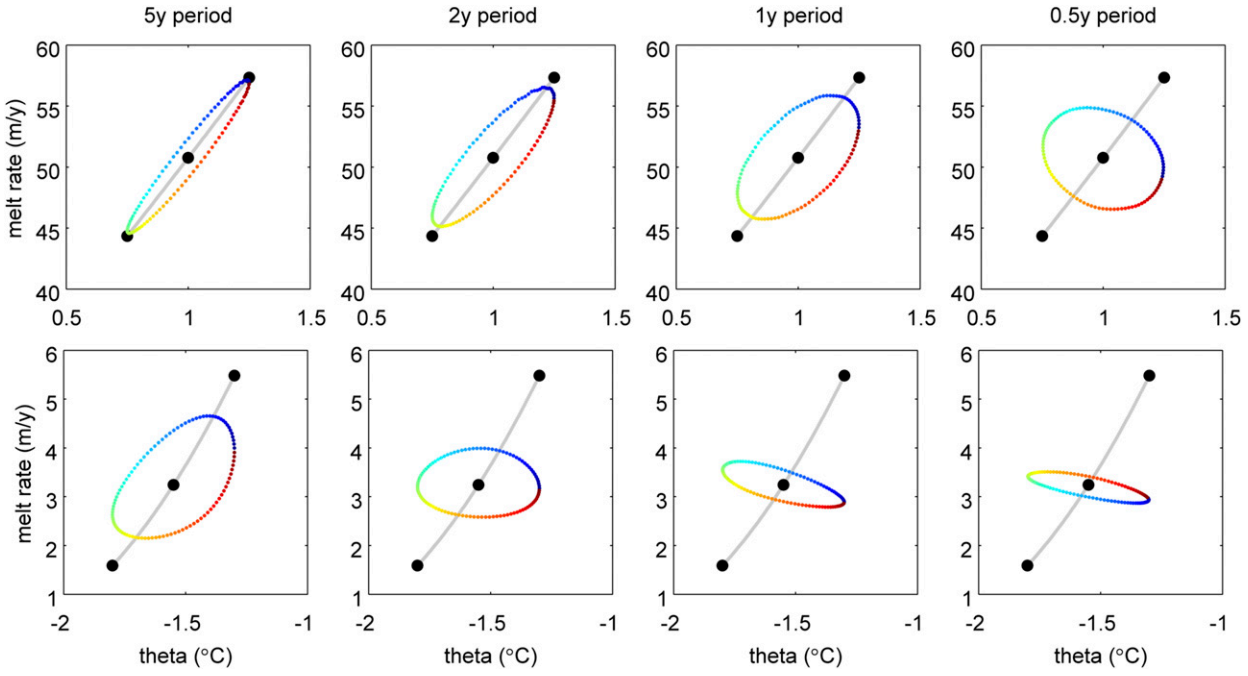

FIG. 8. Equilibrium and transient responses of simulations in the (top) WARM and (bottom) COLD classes. Both classes have a deep-ocean forcing oscillating with an amplitude of 0.5°C, but with the oscillation centered on a different mean temperature. Each column represents a different forcing period for both cases. All panels show the transient response of melting, as in Fig. 5. Warm cases have a higher melt rate, a higher equilibrium sensitivity, and a shorter time scale over which the sensitivity is manifest.

ocean properties (temperature and salinity) and does not consider other forcings such as tides and winds. Furthermore, oscillating far-field ocean conditions are the only external forcing on the system, and this permits an interplay between the residence time controlling the flushing of cavity waters and the cavity water properties controlling the residence time. If the cavity circulation, hence residence time, is instead controlled by other factors, such as wind forcing or sea ice growth offshore of the ice shelf, this feedback is broken. Under these circumstances the warming/cooling asymmetry for intermediate forcing periods may not be expected, since this relies upon the residence time varying through the cycle in response to cavity conditions. The relative sensitivity of warm and cold cavities is also dictated by their residence times and therefore may differ if these

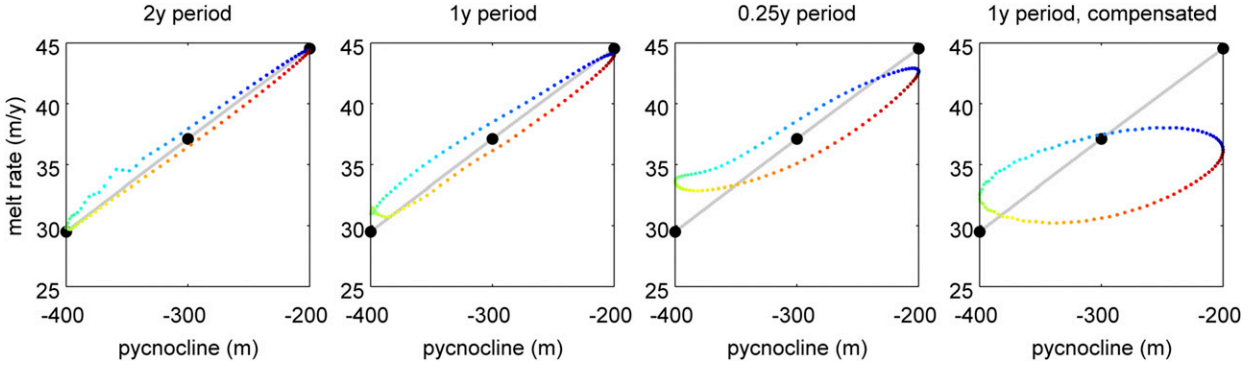

FIG. 9. Equilibrium and transient responses of simulations in the CLINE class. All panels show the transient response of melting, as in Fig. 5. However, in the CLINE class the depth of the pycnocline is oscillated, rather than the deep-ocean conditions. Hence, melting is plotted against the depth of the top of the pycnocline. In the first three panels, the deep-ocean forcing is warm and saline (density is not compensated), so the response of melting to perturbation is extremely rapid. In the last panel, the deep-ocean layer has been freshened such that the density is compensated (i.e., the ocean forcing density is uniform with depth in this case). In this simulation the response is much slower because warm anomalies are not driven into the cavity by their density.

are externally controlled. Finally, the importance of density compensation will change if the circulation is significantly affected by factors other than buoyancy. However, the cavity-driven buoyant circulation is generally important and, whatever the controls on the circulation, it is reasonable to expect that melting anomalies will follow the equilibrium response for variations much slower than the residence time and reduce significantly for variations faster than or equal to the residence time.

It is also important to note that the above results are expressed in terms of the area-mean ice shelf melt rate, which may not be the most relevant metric. For studies concerned with sea level rise, for example, the local melt rate in the shear margins or near the grounding line of an ice shelf may be most important to the buttressing of grounded ice inland. For such studies, the ice-shelf-wide compensation between warm and cold anomalies noted here may be misleading. In addition, larger ice shelf cavities can feature multiple distinct ocean circulations and so could host a range of residence times. This may imply that different sectors of an ice shelf such as FRIS have different sensitivity to transient forcing.

In the simulations, the subice cavity circulation is the limiting factor in propagating ocean anomalies because it is slower than the open-ocean circulation. This generally holds in the real world, where relatively rapid currents in the open ocean are driven by winds and sea ice growth. In some ways this is useful, as it means an ice shelf's sensitivity to forcing can be characterized by considering its local cavity circulation rather than the wider flow in the nearby ocean. However, observing the circulation in an ice shelf cavity is an extremely challenging task.

The mean barotropic cavity residence time is suggested as a key metric of ice shelf sensitivity to unsteady forcing, so it is worth considering how this measure might be derived from observation. Many ice shelf fronts have been sampled with oceanographic sections, which enable an inverse calculation of fluxes into and out of the cavity (e.g., Dutrieux et al. 2014; Jenkins and Jacobs 2008). However, this information can only be used to derive ice front flux residence times, which are shown here to be significantly shorter than the mean cavity measure. In principle, mean cavity residence times can be derived from observations of transient tracers at ice fronts (Loose et al. 2009; Smethie and Jacobs 2005), though detailed knowledge of the ice front flow field is also needed. Residence times have been inferred from measurements within subice cavities (Michel et al. 1979; Nicholls and Østerhus 2004), but this requires both a transient external forcing and knowledge of the cavity flow field. Of course, cavity residence times can be readily calculated from model results, either by area averaging the barotropic streamfunction or using the half-life of a dye tracer (Reddy et al. 2010). Any calculation of residence time remains subject to uncertainty in the volume of the subice cavity, which is significant for many ice shelves. Perhaps the simplest recommendation is that, where possible, all studies state their derived ice front flux and residence time, while modeling studies also report the barotropic cavity residence time.

In the real world, cold-water ice shelves can be an order of magnitude larger than the geometry used in these idealized simulations. (Since melt rates vary over several orders of magnitude, ocean temperatures are an important control on ice shelf extent, and so cold-water ice shelves will be larger if all other factors are equal.) Therefore, real cold-water cavities may have very long residence times, both because their slow melting induces a weak cavity flushing and because the cavity to be flushed is larger. The residence times of the real cold-water ice shelves are estimated at 4–8 years (Loose et al. 2009; Nicholls and Østerhus 2004), an order of magnitude longer than the residence times examined here. There is no reason to believe that the conclusions of this study are inapplicable to larger cavities. This would imply that these large cavities are only sensitive to ocean variation on multiannual time scales and only experience a significant area-mean melting response to multidecadal ocean variation.

6. Conclusions

The *equilibrium response* of ice shelf melting to ocean warming, determined from a set of steady simulations, is that melting varies as a quadratic function of temperature (Holland et al. 2008). This implies that ice shelves forced by warmer water have both higher melt rates and higher sensitivity to ocean temperature change. In this study, unsteady simulations were performed to understand the *transient response* of ice shelf melting to far-field ocean conditions oscillated in time with a variety of periods. The following conclusions are drawn:

1) There is a critical time scale, the subice cavity mean residence time, that dictates the form of the transient response. This residence time is the characteristic time taken for the barotropic circulation to flush the entire subice shelf cavity and is therefore determined by the spatial mean of the barotropic streamfunction. The transient response of ice melting to oscillating ocean forcing is then governed by the relative magnitude of two time scales: the period of oscillation and the mean cavity residence time.

2) If the oscillation period is much longer than the residence time, for example, 10 times longer, the ice shelf cavity is ''fully flushed'' with forcing temperature anomalies at all stages of the forcing cycle. Melting is nearly in equilibrium with the forcing at all times, and melt rates stay close to the equilibrium response.
3) As the oscillation period is decreased, forcing anomalies are no longer fully flushed through the cavity at all times, and melting deviates from the equilibrium response. Importantly, the residence time varies through the forcing cycle. Cold-water cavities have a longer residence time because their meltwater-driven circulation is slow. Thus, as the forcing period is shortened, the residence time during cold cavity conditions is approached first. During the warming phase, the cavity is initially filled with cold water, overturning is slow, and there is a delay in drawing the warm anomaly into the cavity. As a result, the melt rates first deviate from the equilibrium response during the warming phase.
4) When the oscillation period is equal to or less than the residence time, the amplitude of melting anomalies reduces significantly. Cold and warm anomalies coexist in the cavity, and their melting anomalies cancel, providing a relatively steady area-mean melt rate. Reducing the period further simply adds more cancelling anomalies to the cavity. Therefore, for each ice shelf there is a critical cutoff period; variability more rapid than this does not fully affect the shelf-mean melt rate.
5) Ice shelves with a shorter mean residence time are more readily impacted by a given oscillating ocean forcing. First, that oscillation will more readily exceed the (shorter) residence time and thus start to cause melting to vary. Second, that oscillation will exceed the (shorter) residence time by a larger amount and thus induce a larger melting response. Finally, that oscillation will more readily greatly exceed the (shorter) residence time, for example, by 10 times, and hence achieve the full equilibrium response.
6) Ice shelves that are forced by warm water typically have shorter residence times because (i) rapid melting causes a rapid buoyancy-driven circulation and (ii) higher melt rates tend to imply a smaller ice shelf and hence a smaller cavity to be flushed. Therefore, in general, warm-water ice shelves have the highest melt rates, the highest melt rate sensitivity, and the shortest time scale over which that sensitivity is manifest.
7) Ocean temperature changes are usually effected by water mass variations, which implies that they are accompanied by changes in salinity and hence density. The most effective forcing variations have a warm phase that is also saline. The largest deviations from the equilibrium response occur due to a delay originating in the slow, cold-water circulation during the warming phase. When warm anomalies are also saline, buoyancy drives the dense anomaly into the cavity, and the delay is alleviated. When warm anomalies are fresher, they cannot displace the denser, colder water occupying the cavity and the delay is exacerbated.

In summary, the results show that small, warm-water ice shelves subject to warm and saline anomalies are the most sensitive to ocean forcing. These conditions exist in the Amundsen and Bellingshausen Seas. Large, cold-water ice shelves subject to warm and fresh anomalies are least sensitive, and these conditions exist in the Weddell and Ross Seas.

REFERENCES

Christianson, K., and Coauthors, 2016: Sensitivity of Pine Island Glacier to observed ocean forcing. *Geophys. Res. Lett.*, **43**, 10 817–10 825, doi:10.1002/2016GL070500.

Dansereau, V., P. Heimbach, and M. Losch, 2014: Simulation of subice shelf melt rates in a general circulation model: Velocity-dependent transfer and the role of friction. *J. Geophys. Res. Oceans*, **119**, 1765–1790, doi:10.1002/2013JC008846.

De Rydt, J., P. R. Holland, P. Dutrieux, and A. Jenkins, 2014: Geometric and oceanographic controls on melting beneath Pine Island Glacier. *J. Geophys. Res. Oceans*, **119**, 2420–2438, doi:10.1002/2013JC009513.

Determann, J., and R. Gerdes, 1994: Melting and freezing beneath ice shelves: Implications from a three-dimensional ocean-circulation model. *Ann. Glaciol.*, **20**, 413–419, doi:10.3189/172756494794587591.

Dutrieux, P., and Coauthors, 2014: Strong sensitivity of Pine Island Ice-Shelf melting to climatic variability. *Science*, **343**, 174–178, doi:10.1126/science.1244341.

Heimbach, P., and M. Losch, 2012: Adjoint sensitivities of sub-ice-shelf melt rates to ocean circulation under the Pine Island Ice Shelf, West Antarctica. *Ann. Glaciol.*, **53**, 59–69, doi:10.3189/2012/AoG60A025.

Hellmer, H. H., F. Kauker, R. Timmermann, J. Determann, and J. Rae, 2012: Twenty-first-century warming of a large Antarctic ice-shelf cavity by a redirected coastal current. *Nature*, **485**, 225–228, doi:10.1038/nature11064.

Holland, P. R., A. Jenkins, and D. M. Holland, 2008: The response of ice shelf basal melting to variations in ocean temperature. *J. Climate*, **21**, 2558–2572, doi:10.1175/2007JCLI1909.1.

Jacobs, S., A. Jenkins, H. Hellmer, C. Giulivi, F. Nitsche, B. Huber, and R. Guerrero, 2012: The Amundsen Sea and the Antarctic Ice Sheet. *Oceanography*, **25**, 154–163, doi:10.5670/oceanog.2012.90.

Jenkins, A., 2016: A simple model of the ice shelf–ocean boundary layer and current. *J. Phys. Oceanogr.*, **46**, 1785–1803, doi:10.1175/JPO-D-15-0194.1.

——, and S. Jacobs, 2008: Circulation and melting beneath George VI Ice Shelf, Antarctica. *J. Geophys. Res.*, **113**, C04013, doi:10.1029/2007JC004449.

——, H. H. Hellmer, and D. M. Holland, 2001: The role of meltwater advection in the formulation of conservative boundary conditions at an ice–ocean interface. *J. Phys. Oceanogr.*, **31**, 285–296, doi:10.1175/1520-0485(2001)031<0285:TROMAI>2.0.CO;2.

——, K. W. Nicholls, and H. F. J. Corr, 2010: Observation and parameterization of ablation at the base of Ronne Ice Shelf, Antarctica. *J. Phys. Oceanogr.*, **40**, 2298–2312, doi:10.1175/2010JPO4317.1.

——, P. Dutrieux, S. Jacobs, E. J. Steig, G. H. Gudmundsson, J. Smith, and K. J. Heywood, 2016: Decadal ocean forcing and Antarctic Ice Sheet response: Lessons from the Amundsen Sea. *Oceanography*, **29**, 106–117, doi:10.5670/oceanog.2016.103.

Konrad, H., L. Gilbert, S. L. Cornford, A. J. Payne, A. Hogg, A. Muir, and A. Shepherd, 2017: Uneven onset and pace of ice-dynamical imbalance in the Amundsen Sea Embayment, West Antarctica. *Geophys. Res. Lett.*, **44**, 910–918, doi:10.1002/2016GL070733.

Lazeroms, W. M. J., A. Jenkins, G. H. Gudmundsson, and R. S. W. van de Wal, 2017: Modelling present-day basal melt rates for Antarctic ice shelves using a parameterization of buoyant meltwater plumes. *Cryosphere Discuss.*, doi:10.5194/tc-2017-58.

Loose, B., P. Schlosser, W. M. Smethie, and S. Jacobs, 2009: An optimized estimate of glacial melt from the Ross Ice Shelf using noble gases, stable isotopes, and CFC transient tracers. *J. Geophys. Res.*, **114**, C08007, doi:10.1029/2008JC005048.

Losch, M., 2008: Modeling ice shelf cavities in a z coordinate ocean general circulation model. *J. Geophys. Res.*, **113**, C08043, doi:10.1029/2007JC004368.

Makinson, K., P. R. Holland, A. Jenkins, K. W. Nicholls, and D. M. Holland, 2011: Influence of tides on melting and freezing beneath Filchner-Ronne Ice Shelf, Antarctica. *Geophys. Res. Lett.*, **38**, L06601, doi:10.1029/2010GL046462.

Martinson, D. G., S. E. Stammerjohn, R. A. Iannuzzi, R. C. Smith, and M. Vernet, 2008: Western Antarctic Peninsula physical oceanography and spatio–temporal variability. *Deep-Sea Res. II*, **55**, 1964–1987, doi:10.1016/j.dsr2.2008.04.038.

Michel, R. L., T. W. Linick, and P. M. Williams, 1979: Tritium and carbon-14 distributions in seawater from under the Ross Ice Shelf Project Ice Hole. *Science*, **203**, 445–446, doi:10.1126/science.203.4379.445.

Mouginot, J., E. Rignot, and B. Scheuchl, 2014: Sustained increase in ice discharge from the Amundsen Sea Embayment, West Antarctica, from 1973 to 2013. *Geophys. Res. Lett.*, **41**, 1576–1584, doi:10.1002/2013GL059069.

Nicholls, K. W., and S. Østerhus, 2004: Interannual variability and ventilation timescales in the ocean cavity beneath Filchner-Ronne Ice Shelf, Antarctica. *J. Geophys. Res.*, **109**, C04014, doi:10.1029/2003JC002149.

——, L. Boehme, M. Biuw, and M. A. Fedak, 2008: Wintertime ocean conditions over the southern Weddell Sea continental shelf, Antarctica. *Geophys. Res. Lett.*, **35**, L21605, doi:10.1029/2008GL035742.

——, S. Østerhus, K. Makinson, T. Gammelsrød, and E. Fahrbach, 2009: Ice-ocean processes over the continental shelf of the southern Weddell Sea, Antarctica: A review. *Rev. Geophys.*, **47**, RG3003, doi:10.1029/2007RG000250.

Petty, A. A., D. L. Feltham, and P. R. Holland, 2013: Impact of atmospheric forcing on Antarctic continental shelf water masses. *J. Phys. Oceanogr.*, **43**, 920–940, doi:10.1175/JPO-D-12-0172.1.

Reddy, T. E., D. M. Holland, and K. R. Arrigo, 2010: Ross Ice Shelf cavity circulation, residence time, and melting: Results from a model of oceanic chlorofluorocarbons. *Cont. Shelf Res.*, **30**, 733–742, doi:10.1016/j.csr.2010.01.007.

Shepherd, A., D. Wingham, and E. Rignot, 2004: Warm ocean is eroding West Antarctic Ice Sheet. *Geophys. Res. Lett.*, **31**, L23402, doi:10.1029/2004GL021106.

——, and Coauthors, 2012: A reconciled estimate of ice-sheet mass balance. *Science*, **338**, 1183–1189, doi:10.1126/science.1228102.

Smethie, W. M., and S. S. Jacobs, 2005: Circulation and melting under the Ross Ice Shelf: Estimates from evolving CFC, salinity and temperature fields in the Ross Sea. *Deep-Sea Res. I*, **52**, 959–978, doi:10.1016/j.dsr.2004.11.016.

Smith, J. A., and Coauthors, 2016: Sub-ice-shelf sediments record history of twentieth-century retreat of Pine Island Glacier. *Nature*, **541**, 77–80, doi:10.1038/nature20136.

Stern, A. A., D. M. Holland, P. R. Holland, A. Jenkins, and J. Sommeria, 2014: The effect of geometry on ice shelf ocean cavity ventilation: A laboratory experiment. *Exp. Fluids*, **55**, 1719, doi:10.1007/s00348-014-1719-3.

Webber, B. G. M., and Coauthors, 2017: Mechanisms driving variability in the ocean forcing of Pine Island Glacier. *Nat. Commun.*, **8**, 14507, doi:10.1038/ncomms14507.